N20 VIIRS RSB Calibration Algorithms and Results: Collection 2.0

Ning Lei*[a], Kevin Twedt[a], Amit Angal[a], Sherry Li[a], Tiejun Chang[a], Xu Geng[a], and Xiaoxiong Xiong[b]

[a] Science Systems and Applications, Inc., 10210 Greenbelt Road, Lanham, MD, USA 20706
[b]Sciences and Exploration Directorate, NASA Goddard Space Flight Center, Greenbelt, MD, USA 20771
* Corresponding author: ning.lei@ssaihq.com, tel: +1-301-867-2066

ABSTRACT

The NOAA-20 (N20) satellite, previously the Joint Polar Satellite System-1 satellite, was launched on November 18, 2017. One of the five major scientific instruments aboard the satellite is the Visible Infrared Imaging Radiometer Suite (VIIRS). VIIRS scans the Earth's surface in 22 spectral bands, 14 of which are the reflective solar bands (RSBs) with band center wavelengths from 0.412 to 2.25μm. VIIRS regularly performs on-orbit radiometric calibration of its RSBs, primarily through the observations of the onboard solar diffuser (SD). The on-orbit change of the SD's bidirectional reflectance distribution function, known as the H-factor, is determined by the onboard SD stability monitor (SDSM). Since the H-factor exhibits angular dependence, obtaining the H-factor along the SD to the telescope direction is a challenge for the NOAA-20 VIIRS. Recently, Collection 2.0 of the NASA Land Science Investigator-led Processing Systems (SIPS) products were released. As a part of this reprocessing effort, we made two major improvements in the N20 VIIRS RSB radiometric calibration. One is the improved SD and SDSM attenuation screen transmittance functions, obtained by using calibration data collected during both the yaw maneuver and a small portion of regular orbits, resulting in a higher quality H-factor for the SDSM view. Another is the use of the H-factor for the telescope view, derived from the H-factor for the SDSM view, by using the results for the SNPP VIIRS. In June 2019, we delivered a set of mission-long N20 VIIRS Collection 2.0 RSB radiometric calibration look-up-tables. These tables have been employed by the NASA Land SIPS group to reprocess the entire time series of the NOAA-20 VIIRS products. In this paper, we discuss the Collection 2.0 NOAA-20 VIIRS RSB calibration algorithms and results.

1. INTRODUCTION

The Visible Infrared Imaging Radiometer Suite (VIIRS) is a passive cross-track scanning Earth observing sensor.[1] It uses 22 spectral bands to collect photons from 0.41 to 12.50 μm, providing data to generate more than 20 biogeophysical parameters of the Earth, including land, sea, and ice surface temperatures, and aerosol optical thickness and particle size. Each VIIRS band consists of an array of detectors: 16 for the moderate resolution bands (M-bands) and 32 for the imaging bands (I-bands). The M- and I-bands have nadir spatial resolutions of 750 m and 375 m, respectively. Among the 22 bands are the 14 reflective solar bands (RSBs) which detect Earth reflected sunlight from 0.41 to 2.25 μm.

The second VIIRS instrument is aboard the NOAA-20 (N20) satellite, previously known as the Joint Polar Satellite System-1 satellite, launched on November 18, 2017. Like the Suomi National Polar-orbiting Partnership (SNPP) satellite launched on October 28, 2011, the N20 satellite is in a polar orbit with a nominal orbital period of 101.5 min, at an average altitude of 839 km with an equator local crossing time of 13:30 ± 10 min.[2]

Like the SNPP VIIRS, the N20 VIIRS regularly calibrates its RSBs primarily through the observations of the onboard solar diffuser (SD) when the SD is fully illuminated by the Sun.[3] Sunlight reflects off the SD to provide a radiance source to allow for the calibration of the RSBs, as illustrated in Fig. 1. The purpose of the radiometric calibration is to obtain a

factor for each detector of an RSB, known as the F-factor, which is used as a numerical factor to correct the retrieved scene spectral radiance.[4]

However, the SD's bidirectional reflectance distribution function (BRDF) changes its value due to solar exposure in the space environment. The change of the BRDF is represented by a factor known as the H-factor.[4] The onboard SD stability monitor (SDSM) is employed to determine the H-factor,[4,5] by taking the ratio of the signal strengths of the SDSM SD and the Sun views. At the SD view, sunlight passes through the SD screen before striking the SD, and at the Sun view sunlight passes through the SDSM screen before hitting the SDSM. Hence, accurate screen transmittance functions are necessary. Additionally, the H-factor is angle dependent.[6-8] We did not apply the angular dependence for the N20 VIIRS Collection 1.0 RSB radiometric calibration look-up-tables (LUTs), and derived the F-factor using the measured H-factor for the SDSM view without de-convolution of the SDSM detector RSR.

We have addressed the H-factor angular dependence in our previous work for the SNPP VIIRS,[7,9] partly using lunar observation data.[10] But the F-factor derived from the lunar data has a large uncertainty of a few percent or more and unreal large temporal undulations with a peak-to-valley magnitude close to 1%. Due to these undulations, the lunar F-factors of less than three years are not reliable to establish an F-factor temporal trend with sufficient accuracy. To overcome this insufficiency to provide the mission-long RSB F-factor LUTs for the N20 VIIRS Collection 2.0 Level-1B (L1B) products, we have used the relation between the H-factors for the SDSM and telescope views for the SNPP VIIRS. In this paper, we review the algorithms (Section 2) that we have applied for the N20 VIIRS RSB on-orbit radiometric calibration Collection 2.0 and then show the calibration results for the improved screen functions (Section 3) and the H- and F-factors (Section 4).

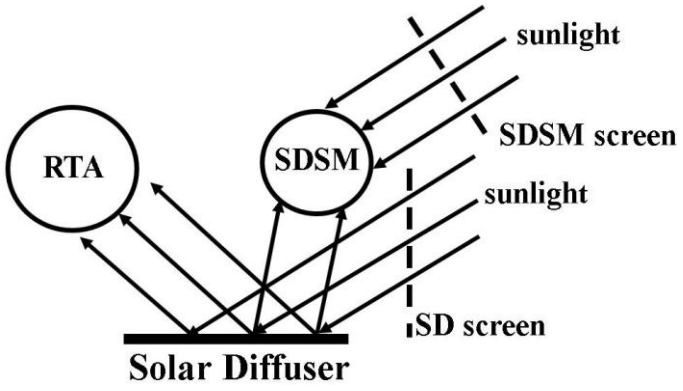


Figure 1. A schematic diagram to illustrate the VIIRS reflective solar band on-orbit radiometric calibration through observations of the onboard sunlit solar diffuser (SD). RTA represents the telescope and SDSM indicates the solar diffuser stability monitor.

2. RSB CALIBRATION ALGORITHMS

Similarly to the SNPP VIIRS,[3] we derive the F-factor using the SD observation data when the SD is fully illuminated by the Sun during a small portion of an orbit near the South Pole over which the ground directly under nadir is still dark. Using L_{SD} to represent the spectral radiance from the sunlit SD, we calculate the F-factor using the following equation[4]

$$F(t,d) = \mathrm{RVS}(\lambda_{\mathrm{B}}, \theta_{\mathrm{SD}}) \times \frac{\int_0^\infty \mathrm{RSR}(\lambda,B) L_{\mathrm{SD}}(\lambda,t) d\lambda}{P(dn_{\mathrm{SD}}) \times \int_0^\infty \mathrm{RSR}(\lambda,B) d\lambda}, \quad (1)$$

where λ_{B} is the band center wavelength, t is time since launch, θ_{SD} is the angle of incidence for the half-angle-mirror (HAM), RVS is the prelaunch reflectivity of the HAM relative to its value when the telescope aims at the center of the space view port, RSR is the prelaunch relative spectral response function of an RSB—an approximation to the modulated

RSR for a detector—since for the N20 VIIRS we have not seen much change in the derived F-factors (see Section 4). In (1), $P(dn_{\mathrm{SD}})$ is a cubic polynomial of dn_{SD} with the coefficients derived from prelaunch values.[11]

The spectral radiance of the sunlit SD, L_{SD}, is given by

$$L_{\mathrm{SD}}(\lambda,t) = \sin\phi_{\mathrm{V,SD}} \times E_{\mathrm{SUN}}(\lambda)\tau_{\mathrm{SD}}\mathrm{BRDF}_{\mathrm{RTA}}\left(\lambda,0,\vec{\phi}\right)H_{\mathrm{RTA}}\left(\lambda,t,\vec{\phi}\right), \quad (2)$$

where $\phi_{\mathrm{V,SD}}$ is the angle between the sunlight and the SD surface, E_{SUN} is the solar spectral irradiance at the VIIRS location with the Thuillier solar spectral power approximation,[12] $\vec{\phi}$ is the solar angle, $\tau_{\mathrm{SD}}\mathrm{BRDF}_{\mathrm{RTA}}$ is the product of the SD screen transmittance and the SD BRDF at the mission start (t=0), and H_{RTA} is the H-factor along the SD-to-telescope direction (the telescope view).

We obtain H_{RTA} using

$$H_{\mathrm{RTA}} = H_{\mathrm{SDSM}} \times \frac{1+\alpha_{\mathrm{RTA}}(\lambda)*(1-H_{\mathrm{SDSM}})}{1+\alpha_{\mathrm{H}}(\lambda)*(1-H_{\mathrm{SDSM}})*(\phi_{\mathrm{H,SD}}^{\mathrm{RTA}}-\phi_{\mathrm{H0}})}, \quad (3)$$

where H_{SDSM} is the SDSM detector RSR de-convoluted H-factor along the SD-to-SDSM direction (the SDSM view), $\phi_{\mathrm{H,SD}}^{\mathrm{RTA}}$ is the solar azimuth angle in the SD coordinate system,[13] and $\phi_{\mathrm{H0}} = 48°$. In (3), the model parameter values are at 2.8/5.2 of the respective values for the SNPP VIIRS.[9] The factor 2.8/5.2 is the ratio obtained for $dH_{\mathrm{SDSM}}/d\phi_{\mathrm{V,SD}}$ (along orbit) for the N20 and the SNPP VIIRS SDs.[14]

We retrieve H_{SDSM} from the ratio of the SDSM detector signal strengths at the SD and Sun views, adjusted by the respective SD and SDSM screen transmittance functions.[4] At a short wavelength infrared (SWIR) band center wavelength, we use a wavelength power law[15] to find H_{SDSM}

$$H_{\mathrm{SDSM}}(\lambda,t) = 1 - \frac{\beta_{\mathrm{H}}(t)}{\lambda^{\eta_{\mathrm{H}}(t)}}, \quad (4)$$

where the model parameters β_{H} and η_{H} are obtained from fitting (4) to the retrieved H_{SDSM} for SDSM detectors 5-8.

To retrieve H_{SDSM}, we need to know the relative product of the SD screen effective transmittance and the BRDF at the mission start, and the SDSM screen's relative effective transmittance. However, the prelaunch measured screen functions are not accurate enough, resulting in large unrealistic undulations in the retrieved measured H_{SDSM} (no RSR de-convolution). Using the approaches that we developed for the SNPP VIIRS,[7,16] we refine the screen functions with calibration data collected during both the yaw maneuver and some regular orbits.[17]

3. IMPROVED SCREEN FUNCTIONS

Based on the experience on the Moderate Resolution Imaging Spectroradiometer,[18] to improve the screen functions, yaw maneuvers were performed for the N20 satellite from orbits 972 to 986. The yaw maneuver data, however, have large gaps in the solar azimuth angles, and hence are unable to resolve the fine features in the screen functions, leading to large unrealistic undulations in the H-factor curves, as shown in Fig. 2.

To resolve the issue shown in Fig. 2, we supplement the yaw maneuver calibration data with the regular calibration data collected between satellite orbits 3291 to 5007. These regular calibration data finely sample the solar azimuth angles and cover the solar angular range expected for the entire mission, allowing us to resolve the fine features in the screen functions, as shown by the triangles, squares, and the solid lines in Fig. 3 for the SDSM screen. The difference in the SDSM screen functions derived from the yaw maneuver data alone and the combined yaw maneuver and regular on-orbit data can reach as large as approximately 1% for SDSM detectors 3 and 4, as shown in Fig. 3. Consequently the SDSM screen function

derived from the combined yaw maneuver and regular on-orbit calibration data improves the H-factors accuracy by as much as approximately 1% for these two detectors.

By adding the regular on-orbit calibration data, the improvement of the relative product of the SD screen effective transmittance and the BRDF for the SDSM view at the mission start is not as large as that for the SDSM screen, as illustrated by Fig. 4, because an SDSM detector is able to view the sunlight that passes through hundreds of through holes on the SD screen.

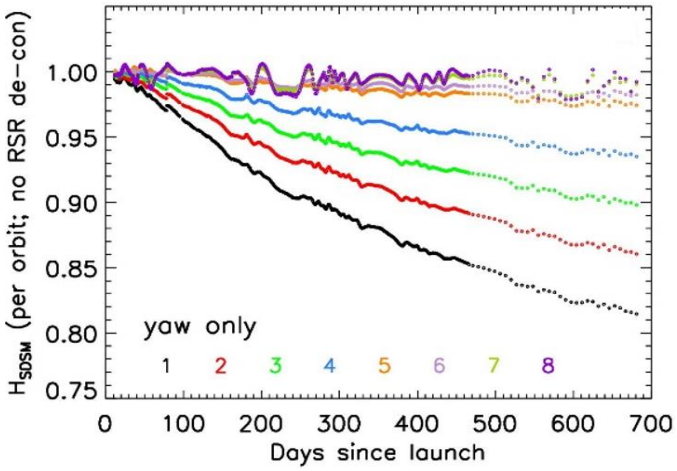


Figure 2. Measured H_{SDSM} (no RSR de-convolution) by using the screen functions refined with only the SDSM calibration data collected on the yaw maneuver orbits.

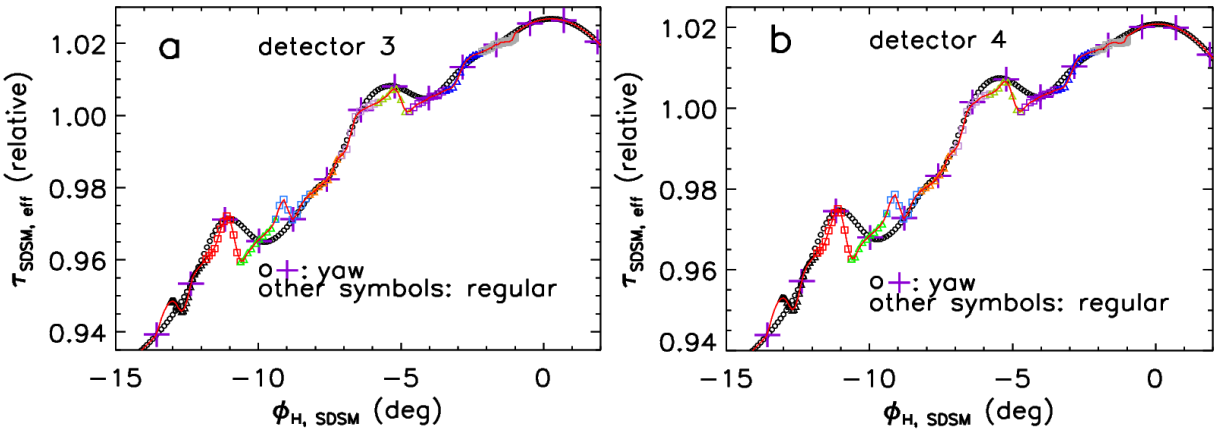


Figure 3. SDSM screen relative effective transmittance at $\phi_{V,SDSM} = 0°$ in the SDSM screen coordinate system,[16] obtained with the calibration data collected on the yaw maneuver orbits only (purple pluses and black circles) and the data collected on both the yaw maneuver orbits and regular satellite orbits 3291 to 5007 (triangles and squares) for the N20 VIIRS SDSM detectors (a) 3 and (b) 4. The circles represent the interpolated transmittance of the values represented by the purple pluses. The solid lines represent the interpolation of the values indicated by the triangles and squares.

From our work on $\tau^{R}_{SD,eff}BRDF_{SDSM}$ (see Fig. 3), we know that adding regular on-orbit calibration data to improve the SD screen function is of minimal improvements. Hence, we use the yaw maneuver data alone to derive the relative product of the SD screen transmittance and the BRDF for the telescope view at t=0. Then we perform a least-squares fit to find the scale factor that multiplies the derived relative product to best match the prelaunch values. The difference between the yaw

maneuver data derived and the prelaunch products of the SD screen transmittance and the BRDF for the telescope view at t=0 is small compared with that for the SNPP VIIRS.[17]

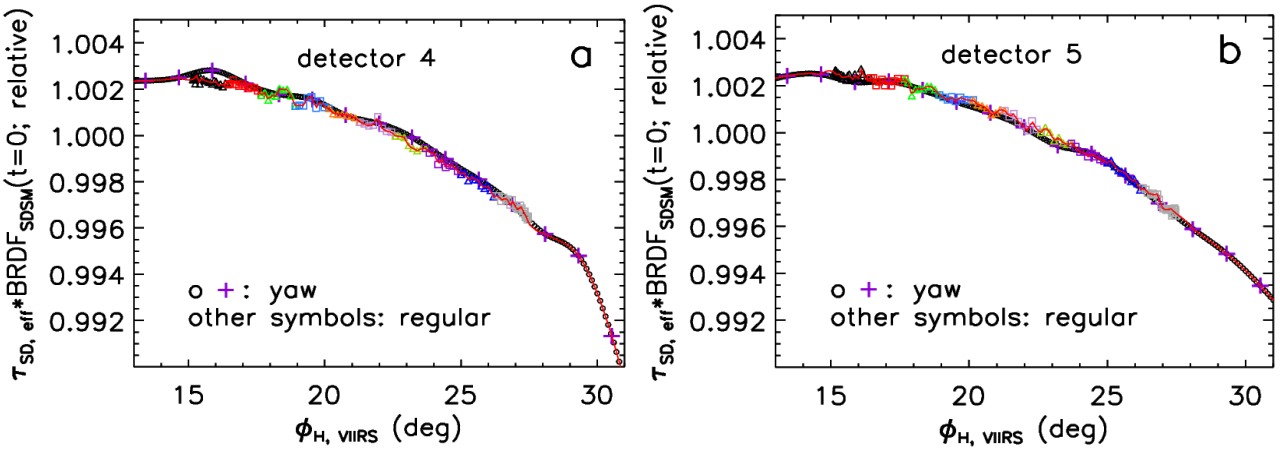


Figure 4. $\tau^{R}_{SD,eff}BRDF_{SDSM}$ vs. the solar azimuth angle $\phi_{H,VIIRS}$ at $\phi_{V,VIIRS} = 16.0°$ in the VIIRS coordinate system[3] for the N20 VIIRS SDSM detectors: (a) 4 and (b) 5. The black circles and purple pluses are from the yaw maneuver data alone, and the red lines and other symbols are from the combined yaw maneuver and regular on-orbit data from orbits 3291 to 5007.

4. RETRIEVED H- AND F-FACTORS

The N20 VIIRS SDSM started nominal operation on satellite orbit 166. To prolong the life of the SDSM, its operation frequency has been reduced in several stages. Currently, the SDSM operates on a small portion of one orbit every Monday.

We first calculate the SDSM detector RSR de-convoluted H-factor, H_{SDSM}. Then we use (3) to retrieve H_{RTA}. By using the improved screen functions illustrated in the last section, the retrieved H_{RTA} is a very smooth function of time, as shown in Fig. 5, compared with the measured H_{SDSM} curves shown in Fig. 2. The smoothness of the curves shown in Fig. 5 is also due to the high signal-to-noise ratios for the SDSM detectors.[14] The H_{RTA} trends downwards generally, as observed for the SNPP VIIRS SD. However, at the same day since launch, the N20 VIIRS H_{RTA} has a larger value (thus less degradation) than the corresponding H_{RTA} for the SNPP VIIRS, as shown in Fig. 5.

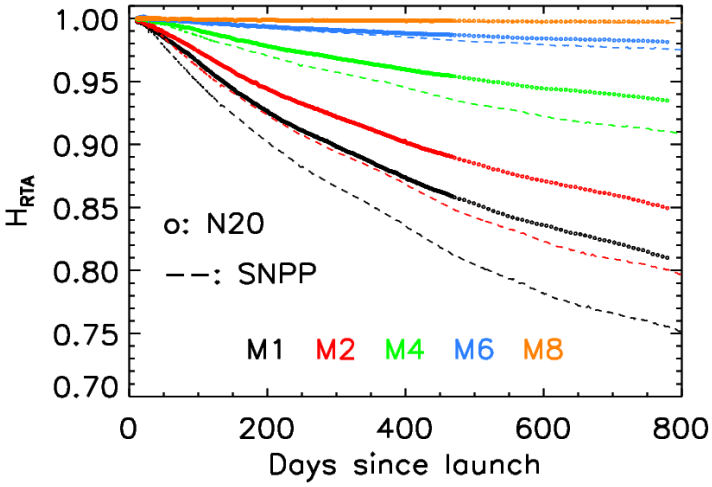


Figure 5. Dots represent H_{RTA} at $\phi_{V,SD} = 35.5°$ for the N20 VIIRS, retrieved by using (3), at the M1, M2, M4, M6, and M8 band center wavelengths. The dashed lines represent the retrieved H_{RTA} at $\phi_{V,SD} = 35.5°$ for the SNPP VIIRS at the respective wavelengths.

The retrieved F-factors do not change significantly with time, varying less than 0.5% for all RSBs since launch. The F-factor trends are especially flat in the time after day 300 in the mission, as illustrated by Fig. 6, a behavior quite different from the SNPP VIIRS where the F-factors trend upwards in time, strongly for bands I2 and M7. It is known that the SNPP VIIRS telescope mirrors were contaminated by tungsten oxides in the prelaunch mirror coating process.[19,20] Exposure of the tungsten oxide thin film to solar UV on orbit causes the film to darken, reducing the reflectivity of the mirrors and increasing the F-factors, with the largest impact seen in the NIR wavelengths. A physical model of the tungsten oxide darkening[21] was successful at describing the general time and wavelength dependence of the measured F-factor changes, suggesting that the darkening effect was the primary cause of the early F-factor degradation for the SNPP VIIRS. The N20 VIIRS did not have any similar mirror contamination and thus it is not surprising that the N20 VIIRS F-factors are much more stable compared with the SNPP VIIRS.

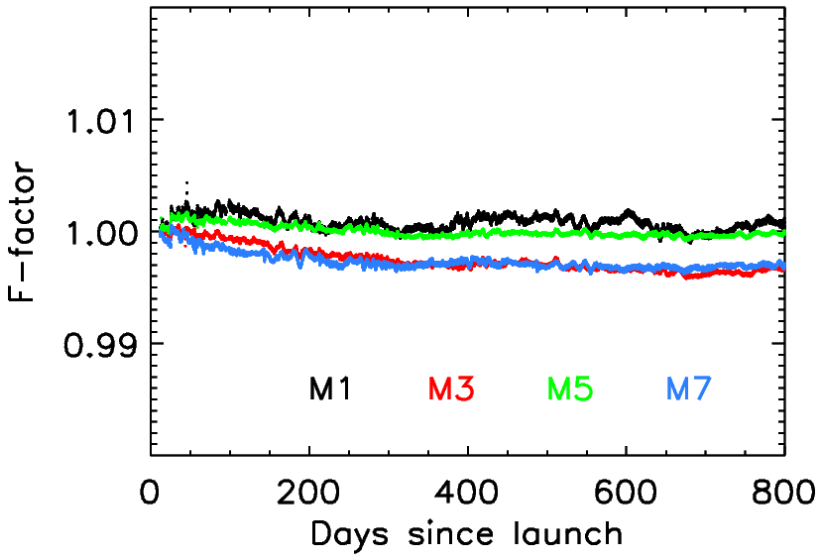


Figure 6. Retrieved SD F-factors, normalized at the first available orbit of 163, for the N20 VIIRS, for bands M1, M3, M5, and M7, at the high-gain stage and averaged over the two HAM sides and all detectors in each band.

5. SUMMARY

In this paper, we have reviewed the algorithms for the N20 VIIRS reflective solar bands on-orbit radiometric calibration Collection 2.0. Using the calibration data collected on both the yaw maneuver and some regular orbits, we have improved the SDSM screen relative effective transmittance and the relative product of the SD screen effective transmittance and the SD BRDF along the SD-to-SDSM direction at the mission start time. We have used the improved screen functions, the SDSM calibration data, and the SDSM detector relative spectral response functions to retrieve the on-orbit BRDF change factor along the SD-to-SDSM direction: H_{SDSM}. We have used an H-factor model that was developed for the SNPP VIIRS to calculate the H-factor along the SD-to-telescope direction, H_{RTA}, from H_{SDSM}. The retrieved N20 VIIRS H_{RTA} are very smooth functions of time, a substantial improvement upon the H-factors derived by using the prelaunch screen functions. At the same wavelength and time in the mission, the N20 VIIRS H_{RTA} are larger (less SD degradation) than the SNPP VIIRS H_{RTA}. We have also refined the relative product of the SD screen transmittance and the BRDF along the SD-to-telescope direction at the mission start, using the calibration data collected on the yaw maneuver orbits. We have retrieved the N20 VIIRS RSB F-factors and showed that the F-factors behave quite differently from those of the SNPP VIIRS: the N20 VIIRS RSB F-factors do not trend significantly upwards nor downwards in time, to within 0.5%, reflecting that the N20 VIIRS telescope mirrors are not contaminated by tungsten oxides that exist on the SNPP VIIRS telescope mirrors.

Finally, we have delivered a set of mission-long N20 VIIRS RSB calibration Collection 2.0 Look-Up-Tables since June 2019 to the NASA Land Science Investigator-led Processing Systems group.

ACKNOWLEDGMENTS

We thank Gal Sarid of the NASA VIIRS characterization support team for review comments.

REFERENCES

[1] Cao, C., De Luccia, F. J., Xiong, X., Wolfe, R., and Weng, F., "Early On-Orbit Performance of the Visible Infrared Imaging Radiometer Suite Onboard the Suomi National Polar-Orbiting Partnership(S-NPP) Satellite," IEEE Trans. Geosci. Remote Sens. 52 (2), 1142-1156, doi: 10.1109/TGRS.2013.2247768 (2014).

[2] Lin, G., Wolfe, R., Tilton, J., Zhang, P., Dellomo, J., and Tan, B., "JPSS-1/NOAA_20 VIIRS early on-orbit geometric performance," Proc. SPIE, 10764, Art ID: 10764-1H, doi: 10.1117/12.2320767 (2018).

[3] Lei, N., Wang, Z., and Xiong, X., "On-orbit Radiometric Calibration of Suomi NPP VIIRS Reflective Solar Bands through Observations of a Sunlit Solar Diffuser Panel," IEEE Trans. Geosci. Remote Sens. 53, 5983-5990, doi: 10.1109/TGRS.2015.2430814 (2015).

[4] Joint Polar Satellite System (JPSS) VIIRS Radiometric Calibration Algorithm Theoretical Basis Document (ATBD); NASA Goddard Space Flight Center: Greenbelt, MD, USA (2013).

[5] Fulbright, J., Lei, N., Efremova, B., and Xiong, X., "Suomi-NPP VIIRS Solar Diffuser Stability Monitor Performance," IEEE Trans. Geosci. Remote Sens. 54, 631-639, doi: 10.1109/TGRS.2015.2441558 (2016).

[6] Lei, N., Chiang, K., and Xiong, X., "Examination of the angular dependence of the SNPP VIIRS solar diffuser BRDF degradation factor," Proc. SPIE 9218, Art ID: 9218-1N (2014).

[7] Lei, N. and Xiong, X., "Products of the SNPP VIIRS SD Screen Transmittance and the SD BRDFs from Both Yaw Maneuver and Regular On-orbit Data," IEEE Trans. Geosci. Remote Sens. 55, 1975-1987 (2017).

[8] Sun, J. and Wang, M., "Visible Infrared Imaging Radiometer Suite solar diffuser calibration and its challenges using a solar diffuser stability monitor," Applied Optics 53, 8571-8584, doi: 10.1364/AO.53.008571 (2014).

[9] Lei, N. and Xiong, X., "Impacts of the Angular Dependence of the Solar Diffuser BRDF Degradation Factor on the SNPP VIIRS Reflective Solar Band On-Orbit Radiometric Calibration," IEEE Trans. Geosci. Remote Sens. 55(3), 1537-1543, doi: 10.1109/TGRS.2016.2626963 (2017).

[10] Xiong, J, Sun, J. Fulbright, Z. Wang, and J. Butler, "Lunar Calibration and Performance for S-NPP VIIRS Reflective Solar Bands," IEEE Trans. Geosci. Remote Sens. 54 (2), 1052-1061, doi: 10.1109/TGRS.2015.2473665 (2016).

[11] Moyer, D., De Luccia, F., and Hass, E., "JPSS-1 VIIRS reflective solar band on-orbit calibration performance impacts due to SWIR nonlinearity artifacts," Proc. SPIE 10000, Art ID: 10000-14; doi: 10.1117/12.2240126 (2016).

[12] Thuillier, G., Herse, M., Labs, D., Foujols, T., Peetermans, W., Gillotay, D., Simon, P. C., and Mandel, H., "The Solar Spectral Irradiance from 200 to 2400 nm as Measured by the SOLSPEC Spectrometer from the Atlas and Eureca Missions," Solar Phys. 214, 1-22 (2003).

[13] Lei, N., Xiong, X., Wang, Z., Li, S., and Twedt, K., "SNPP VIIRS RSB on-orbit radiometric calibration algorithms Version 2.0 and the performances. Part I: The algorithms," submitted to J. of Appl. Rem. Sens., Mar. 2020.

[14] Lei, N., Twedt, K., Xiong, X., and Angal, A., "Early Mission Performance of NOAA-20 VIIRS Solar Diffuser and Solar Diffuser Stability Monitor," submitted to IEEE Trans. Geosci. Remote Sens., Mar. 2020.

[15] Lei, N., and Xiong, X., "Suomi NPP VIIRS Solar Diffuser BRDF Degradation Factor at Short Wave Infrared Band Wavelengths," IEEE Trans. Geosci. Remote Sens. 54, 6212-6216, doi: 10.1109/TGRS.2016.2583220 (2016).

[16] Lei, N., Chen, X., and Xiong, X., "Determination of the SNPP VIIRS SDSM Screen Relative Transmittance from Both Yaw Maneuver and Regular On-Orbit Data," IEEE Trans. Geosci. Remote Sens. 54, 1390-1398, doi: 10.1109/TGRS.2015.2480039 (2016).

[17] Lei, N. and Xiong, X., "Determination of NOAA-20 VIIRS screen transmittance functions with both yaw maneuver and regular on-orbit calibration data," J. Appl. Opt. 59, 2992-3001, doi: 10.1364/AO.386979 (2020).

[18] Xiong, X., Butler, J., Barnes, W., and Guenther, B., "Sensor on-orbit calibration and characterization using spacecraft maneuvers," Proc. IEEE Int. Geosci. Remote Sens. Symp., 2256-2259 (2007).

[19] De Luccia, F., Moyer, D., Johnson, E., Rausch, K., Lei, N., Chiang, K., Xiong, X., Fulbright, J., Hass, E., and Iona, G., "Discovery and characterization of on-orbit degradation of the Visible Infrared Imaging Radiometer Suite (VIIRS) Rotating Telescope Assembly (RTA)," Proc. SPIE 8510, Art ID 8510-1A (2012).

[20] Iona, G., Butler, J. J., Guenther, B., Johnson, E. H., Kennedy, B., Kent, C. J., Lambeck, R. W., Waluschka, E., and Xiong, X., "VIIRS on-orbit optical anomaly: Investigation, analysis, root cause determination and lessons learned," Proc. SPIE 8510, Art ID: 8510-1C (2012).

[21] Lei, N., Xiong, X., and Guenther, B., "Modeling the Detector Radiometric Gains of the Suomi NPP VIIRS Reflective Solar Bands," IEEE Trans. Geosci. Remote Sens. 53, 1565-1573, doi: 10.1109/TGRS.2014.2345481 (2015).